

Neutrino Tomography of Gamma Ray Bursts and Massive Stellar Collapses

Soebur Razzaque,¹ Peter Mészáros¹ and Eli Waxman²

¹*Dpt Astronomy & Astrophysics, Dpt Physics, Pennsylvania State Univ., University Park, PA 16802, USA*

²*Department of Condensed Matter Physics, Weizmann Institute of Science, Rehovot 76100, Israel*

(Dated: March 20, 2022)

Neutrinos at energies above TeV can serve as probes of the stellar progenitor and jet dynamics of gamma ray bursts arising from stellar core collapses. They can also probe collapses which do not lead to gamma-rays, which may be much more numerous. We calculate detailed neutrino spectra from shock accelerated protons in jets just below the outer stellar envelope, before their emergence. We present neutrino flux estimates from such pre-burst jets for two different massive stellar progenitor models. These should be distinguishable by IceCube, and we discuss the implications.

PACS numbers: 96.40.Tv, 98.70.Rz, 98.70.Sa

I. INTRODUCTION

The gamma-ray bursts (GRB) which have so far been accurately localized are associated with regions of active star formation, and their progenitors are thought to be massive stars. The leading model for such bursts involves a relativistic jet, produced following the collapse of the core of the massive stellar progenitor [1]. In this model the γ -rays are produced by synchrotron or inverse Compton radiation from Fermi accelerated electrons in optically thin shocks (see [2] for a review), after the jet has emerged from the stellar envelope. The same optically thin shocks should accelerate relativistic protons [3], and lead to ~ 100 TeV neutrinos via interactions with the observed MeV γ -rays [4]. However, while the jets are still inside the star, shock-accelerated protons can produce \sim TeV neutrinos through photomeson interactions with thermal X-rays in the sub-stellar jet cavity [5].

In this paper we discuss a more general class of massive stellar collapses, in which jet formation may be ubiquitous, but not all of which emerge to be associated with detectable GRBs. Before their successful or failed emergence from the star, the jets can accelerate protons which undergo a more complex sequence of high energy interactions than previously realized. These depend not only on the jet and central engine characteristics but also on the location of the shocks and on the outer dimensions of the stellar progenitor, thus providing potentially useful diagnostics for the type of progenitor as well as the jet and shock parameters. Protons accelerated in sub-stellar jet shocks first undergo photomeson interactions with thermalized shock photons, as well as pp , pn interactions with thermal nucleons in the jet frame. This modifies the relativistic proton spectrum reaching the end of the jet cavity, where the protons undergo a second set of photomeson interactions with stellar X-ray photons and pp , pn interactions with cold nucleons in the stellar frame. The fraction of collapses producing jets which subsequently emerge from the star to produce electromagnetically detectable GRBs are expected to be preceded by a precursor neutrino signal at energies \gtrsim TeV, which is significantly different from the previously calculated $\gtrsim 100$ TeV neutrino signals coincident with the

γ -rays [4]. The fraction of stellar collapses leading to jets which do not emerge would have similar neutrino signals, but they could be more numerous and hence their diffuse flux could be more important.

We discuss our jet models in Sec. II, proton and electron acceleration in the internal shocks in Sec. III and proton interactions in Sec. IV. We discuss neutrino production mechanisms in Sec. V and calculate observed neutrino flux in Sec. VI. We summarize and discuss implications of our results in Sec. VII.

II. COLLAPSAR AND JET MODELS

We take a simplified model for the jet and progenitor star, similar to that described in Ref. [5]. The GRB progenitor is taken to be a massive star with a He core and H envelope. As an example, the parameters chosen are a core radius $r_{\text{He}} \approx 10^{11.5}$ cm, where the density is $\rho_{\text{He}} \sim 10^{-3} \rho_{-3}$ g/cm³. We take two cases, one case (H) where the core is surrounded by an H envelope of size $r_* \sim 10^{13}$ cm, where the density $\rho_{\text{H}} \approx 10^{-7} \rho_{-7}$ g/cm³, and another case (He) where a similar He core has lost its surrounding H envelope. Numerical simulations of collapsar models leading to black hole formation (e.g. [1] indicate that a relativistic jet can be launched along the stellar rotation axis, powered either by thermal $\nu\bar{\nu}$ annihilation or MHD stresses coupling to the black hole and to the debris disk falling back onto the hole). The jet life time is limited by the gas fall-back time onto the black hole, and should be comparable to GRB durations, $\lesssim 10^2$ s. Variability in the effective jet Lorentz factor arises both from variability in the black hole accretion rate, and from instabilities at the jet-stellar interface on the way out from the star.

Internal shocks occur at radii $r_{sh} \sim c\delta t\Gamma^2$ in the highly variable jet outflow, where we expect fluctuations in the bulk Lorentz factor $\Gamma \sim 10^2 - 10^3$ over a wide range of time scales, $0.1\text{ms} \lesssim \delta t \lesssim 1$ s. The observed γ -rays are produced in jet internal shocks between regions with high enough Γ , δt , which occur in the optically thin environment outside the progenitor star (e.g. [2]). Fluctuations with lower Γ , δt are also likely to produce internal shocks

at smaller radii below the stellar surface [5], which will be optically thick. In observed γ -ray light curves, variability on sub-ms timescales is present, the power at high frequencies [6] being subject to Poisson noise uncertainties due to low photon counts. In sub-stellar shocks with smaller lengthscales and Lorentz factors the high frequency power could be relatively more important. Such episodes of lower Γ or shorter variability could arise from instabilities leading to the up and down variation of Γ during propagation of the jet inside the star, as shown in numerical simulations [1].

Here we are interested mainly in these opaque, sub-surface internal shocks. We consider the jets at a time when they are still inside the star, but have advanced to within a factor 1/few of the outer stellar surface. As specific numerical examples we take the internal shock radii at $r_{sh,H} \sim \alpha 10^{12.5} r_{12.5}$ cm and $r_{sh,He} \sim \alpha 10^{11} r_{11}$ cm, where $\alpha \lesssim 0.5$, and the jet termination radii are taken to be $r_{jet,H} \sim 10^{12.5} r_{12.5}$ cm and $r_{jet,He} \sim 10^{11} r_{11}$ cm for the two types of progenitors. The internal shocks at r_{sh} provide a particle accelerator sufficiently far inside the jet cavity, where they are not subject to the large radiative losses in the high photon and nucleon density which are present further out near the jet termination radius r_{jet} , i.e., we consider $r_{sh} < r_{jet} < r_*$. The jets are optically thick to Thomson scattering and the density of photons from the jet termination surface drops off very fast with distance measured inwards into the jet [5]. The shocks in the sub-stellar shocks are likely to be collisionless, since the typical collisionless width $c/\omega_{p,i}$ (where $\omega_{p,i}$ is the ion plasma frequency) is much smaller than the radiation scattering and the particle collision mean free paths. We introduce a parameter ε_{op} that characterizes the fraction of jet energy that is dissipated in the sub-stellar shocks (this energy is given back to the jet, due to the high optical depth, except for the fraction that escapes as neutrino energy). The neutrino fluxes we derive will be proportional to ε_{op} . We cannot estimate ε_{op} directly, since we do not see these collisions. However, it is likely to be significant due to the fluctuations in jet parameters, and we will assume $\varepsilon_{op} \sim 1/2$.

For observed isotropic GRB luminosities $L_\gamma^{iso} = 10^{52} L_{52}$ ergs/s at the termination radius of a sub-surface jet, the jet-frame proton number density is

$$n_{p,jet} = L_\gamma^{iso} / (4\pi r_{jet}^2 \Gamma_{jet}^2 m_p c^3) \approx \begin{cases} 1.8 \times 10^{14} L_{52} r_{12.5}^{-2} \Gamma_{100}^{-2} \text{ cm}^{-3} & \text{(H)} \\ 1.8 \times 10^{17} L_{52} r_{11}^{-2} \Gamma_{100}^{-2} \text{ cm}^{-3} & \text{(He)}. \end{cases} \quad (1)$$

Equating the pressures behind the forward and reverse shocks one finds that the jet head moves at mildly relativistic or subrelativistic speeds with Lorentz factor [8]

$$\Gamma_h \approx \begin{cases} 1.6 L_{52}^{1/4} r_{12.5}^{-1/2} \rho_{-7}^{-1/4} & \text{(H)} \\ 1 L_{52}^{1/4} r_{11}^{-1/2} \rho_{-3}^{-1/4} & \text{(He)}. \end{cases} \quad (2)$$

The number density of protons in the stellar plasma frame is $n_p = 2\Gamma_{jet} n_{p,jet} / \Gamma_h$.

The termination shock where the jet head impacts the star heats up the stellar plasma. The temperature of thermalized shocked photons in the jet head frame, from $L_\gamma^{iso} \approx 4\pi r_{jet}^2 c \Gamma_h^2 a_B T^4$, is

$$T_h \approx \begin{cases} 1.5 L_{52}^{1/4} r_{12.5}^{-1/2} \Gamma_{h,1.6}^{-1/2} \text{ keV} & \text{(H)} \\ 11 L_{52}^{1/4} r_{11}^{-1/2} \Gamma_{h,1}^{-1/2} \text{ keV} & \text{(He)}. \end{cases} \quad (3)$$

The corresponding number density of these photons in the jet head frame, which is approximately the same in the stellar plasma and in the observer's frame, is

$$n_{\gamma,h} = L_\gamma^{iso} / (4\pi r_{jet}^2 \Gamma_h^2 c T_h) \approx \begin{cases} 4.3 \times 10^{23} L_{52}^{3/4} r_{12.5}^{-3/2} \Gamma_{h,1.6}^{-3/2} \text{ cm}^{-3} & \text{(H)} \\ 1.9 \times 10^{26} L_{52}^{3/4} r_{11}^{-3/2} \Gamma_{h,1}^{-3/2} \text{ cm}^{-3} & \text{(He)}. \end{cases} \quad (4)$$

Photons from the shocked stellar plasma diffuse into the jet through Thomson scatterings. Their penetration depth (mean-free path) in the shocked plasma frame is

$$l_\gamma = \Gamma_h / (2\Gamma_{jet} n_{p,jet} \sigma_{Th}) \approx \begin{cases} 6.8 \times 10^7 L_{52}^{-1} r_{12.5}^2 \Gamma_{h,1.6} \Gamma_{100} \text{ cm} & \text{(H)} \\ 3.8 \times 10^4 L_{52}^{-1} r_{11}^2 \Gamma_{h,1} \Gamma_{100} \text{ cm} & \text{(He)}. \end{cases} \quad (5)$$

The density of diffused photons inside the jet head drops off as

$$n_\gamma(x) \approx n_{\gamma,h} e^{-x/l_\gamma} \quad (6)$$

where x is the distance from the jet head radius r_{jet} [5].

III. PARTICLE ACCELERATION

We calculate proton acceleration at the internal shocks which take place at a radius smaller than the termination shock radius ($r_{sh} < r_{jet}$). In principle protons can be accelerated at the termination (forward and reverse) shock too, however, inverse Compton losses significantly reduce the maximum proton energy there [5].

The maximum energy up to which protons are accelerated in the internal shocks is limited by synchrotron losses in the jet magnetic field. (Inverse Compton losses are in the Klein-Nishina limit, [Eq. (17)], and less important than synchrotron). We estimate the magnetic field B_{jet} in the internal shocks, in the jet frame, from the relation $4\pi\alpha^2 r_{sh}^2 c \Gamma_{jet}^2 B_{jet}^2 / 8\pi = \xi_B L_\gamma^{iso}$. Dropping $\alpha \sim 1$ for notational simplicity and assuming a magnetic field equipartition fraction $\xi_B = 10^{-1} \xi_{-1}$, we get

$$B_{jet} \approx \begin{cases} 8.2 \times 10^5 \xi_{-1}^{1/2} L_{52}^{1/2} r_{12.5}^{-1} \Gamma_{100}^{-1} \text{ G} & \text{(H)} \\ 2.5 \times 10^7 \xi_{-1}^{1/2} L_{52}^{1/2} r_{11}^{-1} \Gamma_{100}^{-1} \text{ G} & \text{(He)}. \end{cases} \quad (7)$$

Equating the synchrotron cooling time

$$t_{p,jet}^{syn} = 6\pi m_p^3 / (\sigma_{Th} m_e^2 \gamma_{p,jet} B_{jet}^2) \approx \begin{cases} 7 \times 10^6 \gamma_{p,jet}^{-1} \xi_{-1}^{-1} L_{52}^{-1} r_{12.5}^2 \Gamma_{100}^2 \text{ s} & \text{(H)} \\ 7 \times 10^3 \gamma_{p,jet}^{-1} \xi_{-1}^{-1} L_{52}^{-1} r_{11}^2 \Gamma_{100}^2 \text{ s} & \text{(He)} \end{cases} \quad (8)$$

to the acceleration time

$$\begin{aligned} t_{p,jet}^{acc} &\approx 10(m_p \gamma_{p,jet} / e B_{jet}) \\ &\approx \begin{cases} 1.5 \times 10^{-8} \gamma_{p,jet} \xi_{-1}^{-1/2} L_{52}^{-1/2} r_{12.5} \Gamma_{100} \text{ s} & \text{(H)} \\ 4.7 \times 10^{-10} \gamma_{p,jet} \xi_{-1}^{-1/2} L_{52}^{-1/2} r_{11} \Gamma_{100} \text{ s} & \text{(He)}, \end{cases} \end{aligned} \quad (9)$$

(both evaluated in the jet frame) we get the maximum proton energy in the observer's frame as

$$\begin{aligned} E_p^{max} &= m_p \gamma_{p,jet}^{max} \Gamma_{jet} \\ &\approx \begin{cases} 2.0 \times 10^9 \xi_{-1}^{-1/4} L_{52}^{-1/4} r_{12.5}^{1/2} \Gamma_{100}^{5/2} \text{ GeV} & \text{(H)} \\ 3.6 \times 10^8 \xi_{-1}^{-1/4} L_{52}^{-1/4} r_{11}^{1/2} \Gamma_{100}^{5/2} \text{ GeV} & \text{(He)}. \end{cases} \end{aligned} \quad (10)$$

This is smaller than maximum proton energy achievable in the observed optically thin GRBs, since the internal shocks take place at larger radii in the latter case.

Electrons are also accelerated in the internal shocks, and the average electron energy in the jet frame is $\langle \gamma_e \rangle_{jet} = (m_p/m_e) \varepsilon_e \approx 3.7 \times 10^2 \varepsilon_{0.2}$, where $\varepsilon_e = 0.2 \varepsilon_{0.2}$ is the fraction of thermal energy which goes into electrons. The corresponding peak synchrotron photon energy in the jet frame is $(3/4)(B_{jet}/B_Q) < \gamma_e >_{jet}^2 m_e$, where $B_Q = 4.4 \times 10^{13}$ G. However, the jet is optically thick to Thomson scattering, with an optical depth in the jet frame, from Eq. (1), of

$$\tau_{Th,jet} = \frac{\sigma_{Th} n_{p,jet} r_{sh}}{\Gamma_{jet}} \approx \begin{cases} 4 L_{52} r_{12.5}^{-1} \Gamma_{100}^{-3} & \text{(H)} \\ 120 L_{52} r_{11}^{-1} \Gamma_{100}^{-3} & \text{(He)}. \end{cases} \quad (11)$$

Note that these values for sub-stellar jets are larger than those in the internal shocks responsible for γ -rays outside the star, due to the smaller distances and higher densities. Hence the synchrotron photons thermalize to an approximate black-body temperature of

$$\begin{aligned} E_{\gamma,jet}^{syn} &= [L_{\gamma}^{iso} / (4\pi r_{sh}^2 \Gamma_{jet}^2 c a_B)]^{1/4} \\ &\approx \begin{cases} 0.2 L_{52}^{1/4} r_{12.5}^{-1/2} \Gamma_{100}^{-1/2} \text{ KeV} & \text{(H)} \\ 1.2 L_{52}^{1/4} r_{11}^{-1/2} \Gamma_{100}^{-1/2} \text{ KeV} & \text{(He)} \end{cases} \end{aligned} \quad (12)$$

in the jet frame. The corresponding number density of synchrotron photons in the jet frame is

$$\begin{aligned} n_{\gamma,jet}^{syn} &= L_{\gamma}^{iso} / (4\pi r_{sh}^2 \Gamma_{jet}^2 c E_{\gamma,jet}^{syn}) \\ &\approx \begin{cases} 8.0 \times 10^{20} L_{52}^{3/4} r_{12.5}^{-3/2} \Gamma_{100}^{-3/2} \text{ cm}^{-3} & \text{(H)} \\ 1.4 \times 10^{23} L_{52}^{3/4} r_{11}^{-3/2} \Gamma_{100}^{-3/2} \text{ cm}^{-3} & \text{(He)}. \end{cases} \end{aligned} \quad (13)$$

We have also calculated energy losses by the protons due to photopair and photomeson interactions with synchrotron photons, which could possibly limit their acceleration. The Bethe-Heitler process $p\gamma \rightarrow pe^+e^-$ has a very large cross-section of $\approx 5 \times 10^{-25} \text{ cm}^2$ at threshold, but the energy lost by the proton is negligible (although they might play a role in more accurate calculations of the asymptotic energy losses). Photomeson interactions affect proton acceleration at energies only above Δ production threshold, which we discuss in the following section. The typical jet crossing time in the comoving frame:

$30/100 \sim 0.3$ s, for bulk Lorentz factor $\Gamma = 100$, is much longer than the acceleration time in Eq. (9) for all but the highest proton energies achievable. Hence the jet crossing time does not introduce any additional constraints for protons to accelerate to the maximum observer-frame energies of Eq. (10), leading to a similar upper limit.

IV. PROTON INTERACTIONS

High energy protons accelerated in the sub-stellar internal shocks undergo $p\gamma$ and pp interactions both inside the jet and near its termination boundary with the stellar envelope. We discuss each case below.

Protons first interact inside the jet with synchrotron photons from co-accelerated electrons, and with the fraction of jet protons which are not accelerated at the internal shocks. The dominant inelastic channel is $p\gamma \rightarrow \Delta$ with $\approx 5 \times 10^{-28} \text{ cm}^2$ cross-section ($\sigma_{p\gamma \rightarrow \Delta}$) and $\approx 20\%$ inelasticity. The $p\gamma$ optical depth at the Δ resonance from Eq. (13) in the jet frame is then

$$\begin{aligned} \tau_{p\gamma,jet}^{syn} &= (\sigma_{p\gamma \rightarrow \Delta} n_{\gamma,jet}^{syn} r_{sh} / \Gamma_{jet}) \\ &\approx \begin{cases} 1.3 \times 10^4 L_{52}^{3/4} r_{12.5}^{-1/2} \Gamma_{100}^{-5/2} & \text{(H)} \\ 7.0 \times 10^4 L_{52}^{3/4} r_{11}^{-1/2} \Gamma_{100}^{-5/2} & \text{(He);} \end{cases} \end{aligned} \quad (14)$$

very large in both cases (see e.g. [7] for photomeson interactions in a different, optically thin, GRB acceleration scenario). With an optical depth so large, high energy protons lose all their energies through $p\gamma$ interactions. Secondary neutrons produced in the subprocess $p\gamma \rightarrow \Delta \rightarrow n\pi^+$ also undergo photo-meson processes just like protons. This scenario is different from that of optically thin shocks in observed GRBs, where the $p\gamma$ optical depth is much smaller because of larger shock radii [4, 9]. The threshold proton energy for $p\gamma$ interaction at the Δ resonance, from the condition $E_p^{th} E_{\gamma,jet}^{syn} \approx 0.3 \Gamma_{jet}^2 \text{ GeV}^2$, in the observer's frame, from Eq. (12), is

$$E_{p,th}^{syn} \approx \begin{cases} 1.5 \times 10^8 L_{52}^{-1/4} r_{12.5}^{1/2} \Gamma_{100}^{3/2} \text{ GeV} & \text{(H)} \\ 2.5 \times 10^7 L_{52}^{-1/4} r_{11}^{1/2} \Gamma_{100}^{3/2} \text{ GeV} & \text{(He);} \end{cases} \quad (15)$$

approximately an order of magnitude below the maximum proton energy given in Eq. (10). Due to the smaller (sub-stellar) radii of these shocks and the different target photons, the optical depths and threshold proton energies are respectively higher and lower than those [4] in γ -ray producing shocks outside the stars.

Next, we consider pp interactions in the internal shocks. Typically a fraction $\zeta_p < 1$ of the protons are Fermi accelerated in the internal shocks of the GRB jet. The remaining fraction $(1 - \zeta_p)$ of cold protons provide targets for pp interactions. The mean total cross-section for pp interactions in the TeV-PeV energy range is $\langle \sigma_{pp} \rangle \approx 6 \times 10^{-26} \text{ cm}^2$. The corresponding optical depth in the jet frame, from Eq. (1), is

$$\langle \tau_{pp} \rangle_{jet} = (1 - \zeta_p) n_{p,jet} \langle \sigma_{pp} \rangle r_{sh} / \Gamma_{jet}$$

$$\approx \begin{cases} 0.3(1 - \zeta_p)L_{52}r_{12.5}^{-1}\Gamma_{100}^{-3} & \text{(H)} \\ 11(1 - \zeta_p)L_{52}r_{11}^{-1}\Gamma_{100}^{-3} & \text{(He)}; \end{cases} \quad (16)$$

much smaller than $p\gamma$ optical depth. At energies well below the maximum proton energies, the competing effect of inverse Compton (IC) scattering reduces the pp scattering rate significantly, because of the large synchrotron photon density in the internal shocks.

The cross-section for inverse Compton is $\sigma_{\text{IC}} \approx \sigma_{\text{Th}}(m_e/m_p)^2$ in the non-relativistic Thomson limit. The Thomson limit applies when $E_\gamma E_p/m_p^2 \ll 1$ in the co-moving frame. Solving for the synchrotron photon energies [Eq. (12)] in the $r_{12.5}$ and r_{11} cases, the Thomson limits are valid for $E_{p,jet}^{\text{IC}} \lesssim 4 \times 10^6$ GeV and 7×10^5 GeV respectively in the jet frame. The same quantity in the observer's frame

$$E_p^{\text{IC}} \lesssim \begin{cases} 4 \times 10^8 L_{52}^{-1/4} r_{12.5}^{1/2} \Gamma_{100}^{3/2} \text{ GeV} & \text{(H)} \\ 7 \times 10^7 L_{52}^{-1/4} r_{11}^{1/2} \Gamma_{100}^{3/2} \text{ GeV} & \text{(He)}; \end{cases} \quad (17)$$

is higher than $E_{p,th}^{\text{syn}}$ [Eq. (15)]. The ratio of IC to pp optical depth for the two internal shock radii is

$$\frac{\tau_{\text{IC},jet}}{\langle \tau_{pp} \rangle_{jet}} = \frac{n_{\gamma,jet}^{\text{syn}} \sigma_{\text{Th}} (m_e/m_p)^2}{n_{p,jet} \langle \sigma_{pp} \rangle} \approx \begin{cases} 14.6 L_{52}^{-1/4} r_{12.5}^{1/2} \Gamma_{100}^{1/2} & \text{(H)} \\ 2.6 L_{52}^{-1/4} r_{11}^{1/2} \Gamma_{100}^{1/2} & \text{(He)}. \end{cases} \quad (18)$$

The proton flux is suppressed according to Eq. (18) below E_p^{IC} for pp interactions in the internal shocks. In the ultra-relativistic Klein-Nishina limit: $E_\gamma E_p/m_p^2 \gg 1$, the pp optical depth becomes larger than the IC optical depth with increasing proton energy. However $p\gamma$ interactions are dominant above $E_{p,th}^{\text{syn}}$ anyway.

Protons below $E_{p,th}^{\text{syn}}$ in the r_{11} case, undergo pp interactions in the internal shocks with reduced flux [Eq. (18)]. In the $r_{12.5}$ case, most protons below $E_{p,th}^{\text{syn}}$ escape the internal shocks to interact with shocked photons in the jet head and cold stellar protons. We discuss these interactions below.

The threshold proton energy at the Δ resonance for $p\gamma$ interactions with shocked photons in the jet head, from Eq. (3), is

$$E_{p,th}^{\text{sh}} = 0.3 \Gamma_h / T_h \approx 3.2 \times 10^5 L_{52}^{-1/4} r_{12.5}^{1/2} \Gamma_{h,1.6}^{3/2} \text{ GeV} \quad \text{(H)} \quad (19)$$

in the observer's frame. The corresponding optical depth, in the jet head frame, depends on the photon number density given in Eq. (6) as

$$\tau_{p\gamma}^{\text{sh}}(x) = l_\gamma / l_{p\gamma}(x) \approx l_\gamma (\sigma_{p\gamma \rightarrow \Delta}) n_{\gamma,h} e^{-x/l_\gamma} \approx 1.46 \times 10^4 e^{-x/l_\gamma} \times L_{52}^{-1/4} r_{12.5}^{1/2} \Gamma_{h,1.6}^{-1/2} \Gamma_{100} \quad \text{(H)}. \quad (20)$$

Since protons lose 20% of their energy in each $p\gamma$ interaction, it takes about 5 optical depths for a proton of

energy $E_{p,th}^{\text{syn}}$ in Eq. (15) to fall below $E_{p,th}^{\text{sh}}$. Solving Eq. (20) for x and $\tau_{p\gamma}^{\text{sh}}(x) = 5$, we have $x/l_\gamma \approx 8$. The shocked photon density at this distance, from Eq. (4), is then

$$n_\gamma^{\text{sh}} \approx 1.4 \times 10^{20} L_{52}^{3/4} r_{12.5}^{-3/2} \Gamma_{h,1.6}^{-3/2} \text{ cm}^{-3} \quad \text{(H)} \quad (21)$$

in the jet head.

Protons below $E_{p,th}^{\text{sh}}$ in the $r_{12.5}$ case, interact with cold stellar protons in the H envelope. The number density of stellar protons is $n_{p,H} \approx 6 \times 10^{16} \text{ cm}^{-3}$. The corresponding pp optical depth for cold stellar protons in the stellar plasma frame is

$$\langle \tau_{pp} \rangle_* = \langle \sigma_{pp} \rangle n_{p,H} (r_* - r_{jet}) \approx 2.5 \times 10^4 \quad (22)$$

which is very large and forces all protons to undergo pp interactions.

V. NEUTRINO PRODUCTION

High energy neutrinos are produced both in $p\gamma$ and pp interactions dominantly through secondary pion (π^\pm) decays as $\pi^\pm \rightarrow \mu\nu_\mu \rightarrow e\nu_e\nu_\mu\bar{\nu}_\mu$. Each of the secondary leptons share roughly 1/4 of the initial pion energy.

Because of the high $p\gamma$ optical depth in the internal shocks [Eq. (14)], pions and muons are produced in the thermalized synchrotron photon bath. The high magnetic field and synchrotron photon density in the shocks may force high energy pions and muons, from $p\gamma$ interactions, to lose their energies through synchrotron radiation and inverse Compton scatterings before they decay to neutrinos. The same is true for $p\gamma$ interactions with photons from the shocked plasma in the jet head for the $r_{12.5}$ case. Neutrinos from pp interactions taking place outside the jet head in the unshocked stellar plasma, however, are not affected because of the much smaller magnetic field and photon density in the plasma. We discuss synchrotron and inverse Compton losses in the GRB jet below.

The synchrotron loss time for pions and muons in the jet frame can be calculated using formulae similar to Eq. (8) for protons. Equating this time to the particle decay time in the jet frame, $\tau_{\pi,jet}^{\text{dec}} = 2.6 \times 10^{-8} \gamma_{\pi,jet}$ s and $\tau_{\mu,jet}^{\text{dec}} = 2.2 \times 10^{-6} \gamma_{\mu,jet}$ s, we get the maximum synchrotron break energies, in the observer's frame: $E_{\pi;\mu,jet}^{\text{sb}} = m_{\pi;\mu} \gamma_{\pi;\mu,jet}^{\text{max}} \Gamma_{jet}$, as

$$E_\pi^{\text{sb}} \approx \begin{cases} 1.3 \times 10^7 \xi_{-1}^{-1/2} L_{52}^{-1/2} r_{12.5} \Gamma_{100} \text{ GeV} & \text{(H)} \\ 4.2 \times 10^5 \xi_{-1}^{-1/2} L_{52}^{-1/2} r_{11} \Gamma_{100} \text{ GeV} & \text{(He)} \end{cases} \quad (23)$$

for pions and

$$E_\mu^{\text{sb}} \approx \begin{cases} 7.0 \times 10^5 \xi_{-1}^{-1/2} L_{52}^{-1/2} r_{12.5} \Gamma_{100} \text{ GeV} & \text{(H)} \\ 2.2 \times 10^4 \xi_{-1}^{-1/2} L_{52}^{-1/2} r_{11} \Gamma_{100} \text{ GeV} & \text{(He)} \end{cases} \quad (24)$$

for muons.

The inverse Compton (IC) losses are more severe for muons than for pions. The IC cooling time for a particle of mass m_i in the Thomson and Klein-Nishina (KN) limits is

$$\begin{aligned} t_{i,jet}^{\text{IC,Th}} &= \frac{m_i}{\sigma_{\text{Th}} c \gamma_{i,jet} E_{\gamma,jet} n_{\gamma,jet}} ; \gamma_{i,jet} \ll \frac{m_i}{E_{\gamma,jet}} \\ t_{i,jet}^{\text{IC,KN}} &= \frac{\gamma_{i,jet} (E_{\gamma,jet}/m_i)}{\sigma_{\text{Th}} (m_e/m_i)^2 c n_{\gamma,jet}} ; \gamma_{i,jet} \gg \frac{m_i}{E_{\gamma,jet}} \end{aligned} \quad (25)$$

respectively in the jet frame. The ratio of IC cooling time to the particle decay time, for synchrotron photons from Eqs. (12 & 13), in the Klein-Nishina limit, is

$$\frac{t_{\pi,jet}^{\text{IC,syn}}}{\tau_{\pi,jet}^{\text{dec}}} \approx \begin{cases} 2.6 \times 10^{-1} L_{52}^{-1/2} r_{12.5} \Gamma_{100}; & \gamma_{\pi,jet} \gtrsim 7 \times 10^5 \\ 8.9 \times 10^{-3} L_{52}^{-1/2} r_{11} \Gamma_{100}; & \gamma_{\pi,jet} \gtrsim 10^5 \end{cases} \quad \begin{matrix} \text{(H)} \\ \text{(He)} \end{matrix} \quad (26)$$

for pions and

$$\frac{t_{\mu,jet}^{\text{IC,syn}}}{\tau_{\mu,jet}^{\text{dec}}} \approx \begin{cases} 2.3 \times 10^{-3} L_{52}^{-1/2} r_{12.5} \Gamma_{100}; & \gamma_{\mu,jet} \gtrsim 5 \times 10^5 \\ 7.9 \times 10^{-5} L_{52}^{-1/2} r_{11} \Gamma_{100}; & \gamma_{\mu,jet} \gtrsim 9 \times 10^4 \end{cases} \quad \begin{matrix} \text{(H)} \\ \text{(He)} \end{matrix} \quad (27)$$

for muons. As a result, above $\gamma_{\pi;\mu,jet} \approx m_{\pi;\mu}/E_{\gamma,jet}$, only $\approx 26\%$ of the pions produced by $p\gamma$ interactions in the internal shocks, in the $r_{12.5}$ case, decay to ν_μ . Production of ν_e and $\bar{\nu}_\mu$, from μ -decay, in the $r_{12.5}$ case is suppressed by IC losses. All flavors of neutrino production in the internal shocks from $p\gamma$ interactions is suppressed in the r_{11} case by IC losses. Below $\gamma_{\pi;\mu,jet} \approx m_{\pi;\mu}/E_{\gamma,jet}$ neutrino production is suppressed as E_ν^{-2} due to IC losses in the Thomson limit. Similarly, for pp interactions in the internal shocks, neutrino production is also suppressed by IC losses.

Neutrino production with the shocked photons in the jet head, in the $r_{12.5}$ case, is also affected by inverse Compton losses. The decay length $c\tau_{\pi;\mu}$ in the shocked plasma frame exceeds the shocked photon penetration depth [Eq. (5)] for $\gamma_\pi \gtrsim 9 \times 10^4$ and $\gamma_\mu \gtrsim 10^3$. As a result pions and muons produced in the $p\gamma$ interactions “see” an increasing photon density according to Eq. (6). For simplicity we compute the ratios of IC loss times to the decay times for pions and muons, in the Klein-Nishina limit: $\gamma_\pi \gtrsim 9 \times 10^4$ and $\gamma_\mu \gtrsim 6 \times 10^4$, as

$$\begin{aligned} t_{\pi}^{\text{IC,sh}}/\tau_{\pi}^{\text{dec}} &\approx 3.6 \times 10^{-3} L_{52}^{-1/2} r_{12.5} \Gamma_{h,1.6} \quad \text{(H)} \\ t_{\mu}^{\text{IC,sh}}/\tau_{\mu}^{\text{dec}} &\approx 3.2 \times 10^{-5} L_{52}^{-1/2} r_{12.5} \Gamma_{h,1.6} \quad \text{(H)} \end{aligned} \quad (28)$$

using Eqs. (3 & 4). As a result, all flavors of neutrino production is suppressed by IC losses in the jet head.

VI. NEUTRINO FLUX CALCULATION

The proton energy distribution in the sub-stellar internal shocks, in the observer frame, is given by

$$\frac{d^2 N}{dE_p dt} = \frac{\zeta_p \varepsilon_{\text{op}} L_{\gamma}^{\text{iso}}}{E_p^2} \approx 6 \times 10^{54} \frac{\zeta_p \varepsilon_{\text{op}} L_{52}}{E_p^2} \text{GeV}^{-1} \text{s}^{-1}, \quad (29)$$

where ζ_p is the injection fraction of protons into the acceleration process and ε_{op} is the fraction of jet energy dissipated in sub-surface shocks (whose order of magnitude is $\sim 1/2$). The neutrino flux, the same for ν_μ , ν_e and $\bar{\nu}_\mu$ in the pp and $p\gamma$ interactions, from a single GRB buried jet at a distance D is [10]

$$\begin{aligned} \Phi_\nu &= d^2 N / dE_\nu dt = 1/4\pi D^2 \\ &\times \begin{cases} \int f_{pp} M_\nu(E_p) \frac{d^2 N}{dE_p dt} dE_p & ; E_p \lesssim E_p^{\text{th}} \\ (f_\pi/4) \frac{d^2 N}{dE_p dt} & ; E_p > E_p^{\text{th}} \end{cases} \end{aligned} \quad (30)$$

where $f_{pp} = \min(1, <\tau_{pp}>)$ and $f_\pi = \min(1, \tau_{p\gamma})$ from Eqs. (16 & 14) respectively. We have used the PYTHIA 6.2 event generator [11], widely used in high energy particle physics, to simulate pp interactions. For our problem, the neutrino multiplicity, through pion decay, in the pp interactions can be written as [10]

$$\begin{aligned} M_\nu(E_p) &= \frac{7}{4} \left(\frac{E_\nu}{\text{GeV}} \right)^{-1} \left[\frac{1}{2} \ln \left(\frac{10^{11} \text{ GeV}}{E_p} \right) \right]^{-1} \\ &\times \Theta \left(\frac{1}{4} \frac{m_\pi}{\text{GeV}} \gamma_{\text{CM}} \leq \frac{E_\nu}{\text{GeV}} \leq \frac{1}{4} \frac{E_p}{\text{GeV}} \right) \end{aligned} \quad (31)$$

for each flavor of neutrino. However, observed neutrino fluxes, for different flavors, are greatly affected by the environments at which they are produced. We discuss our flux calculation method next.

In the r_{11} (He) case, all flavors of neutrinos produced from $p\gamma$ and pp interactions are heavily suppressed by inverse Compton losses both in the Thomson and Klein-Nishina limits [Eqs. (26 & 27)]. We have calculated the muon neutrino flux (see Fig. 1) from pp interactions below $E_{p,th}^{\text{syn}}$ [Eq. (15)], in the internal shocks, using $\sim 40\%$ of the proton flux [Eq. (29)] according to Eq. (18). Above $E_{p,th}^{\text{syn}}$ (corresponding to $E_\nu \sim 10^{6.5}$ GeV) we used the full proton flux to calculate neutrino flux from $p\gamma$ interactions (not shown in the figure).

The $r_{12.5}$ (H) case is more complicated. Below $E_{p,th}^{\text{sh}}$ (Eq. [19], corresponding to $E_\nu \sim 10^{4.5}$ GeV), we calculate neutrino flux through pp interactions with cold stellar protons in the H envelope. We used $\sim 70\%$ of the proton flux [Eq. (29)] escaping the internal shocks according to Eq. (16) for this calculation. Note that neutrinos thus produced in the H envelope are not suppressed by inverse Compton losses. Above $E_{p,th}^{\text{sh}}$ and below $E_{p,th}^{\text{syn}}$ [Eq. (15)] ν_μ production from $p\gamma$ interactions, at the jet head, is suppressed by IC losses [Eq. (28)]. Similar IC suppression [Eqs. (26 & 27)] applies for ν 's from $p\gamma$, in the internal shocks, above $E_{p,th}^{\text{syn}}$. An extra

reduction of the flux happens above E_π^{sb} [Eq. 23] due to synchrotron radiation by pions.

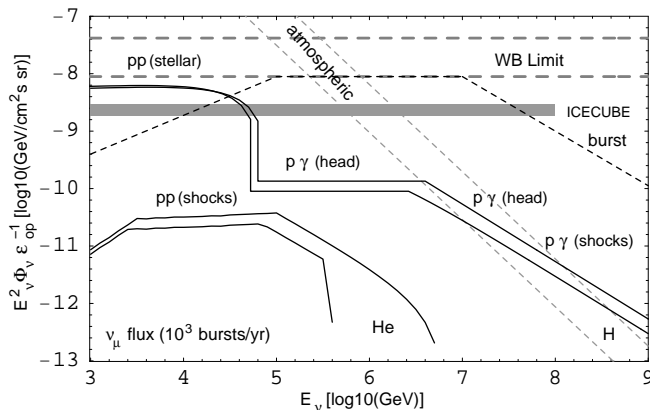


FIG. 1: Diffuse muon-neutrino flux $E_\nu^2 \Phi_\nu \epsilon_{op}^{-1}$, shown as solid lines, from sub-stellar jet shocks in two GRB progenitor models, H ($r_{12.5}$) and He (r_{11}), each for two sets of shock/jet radii and overlying envelope masses (with similar curves for ν_μ , ν_e and ν_τ). These neutrinos arrive as precursors (10-100 s before) of γ -ray bright (electromagnetically detectable) bursts, or as the sole signal in the case of γ -ray dark bursts. Also shown is the diffuse neutrino flux arriving simultaneously with the γ -rays from shocks outside the stellar surface in observed GRB (dark short-dashed curve); the Waxman-Bahcall (WB) diffuse cosmic ray bound (light long-dashed curves); and the atmospheric neutrino flux (light short-dashed curves). For a hypothetical 100:1 ratio of γ -ray dark (in which the jets do not emerge) to γ -ray bright collapses, the neutrino fluxes would be 100 times higher than those plotted here.

The diffuse ν_μ flux levels are shown in Fig. 1 as solid curves for the H (upper two curves) and He (lower two curves) star models. The nominal set of jet and shock radii discussed in §II and above ($\alpha \sim 1$, H: $r_{12.5}$ and He: r_{11}) give the uppermost solid curve of each set. For comparison, we also show the flux for a different choice of jet and shock radii, plotted as the lower of each set of solid curves; these latter have $r_{jet,H} \sim 10^{12.3}$ cm, $r_{sh,H} \sim 10^{12}$ cm in the H case, and $r_{jet,He} \sim 10^{10.8}$ cm and $r_{sh,He} \sim 10^{10.5}$ cm in the He case respectively. Note that, because of a pp component, the neutrino flux we calculated is higher in the < 100 TeV range compared to optically thin shocks [4, 9]. As a result, one gets more events in a neutrino detector than one would from optically thin shocks [12].

The effects of absorption by νN interactions in the overlying stellar envelope at the highest energies plotted in Fig. 1 are calculated using the cross sections [13] and the overlying grammages above the jet head. The absorption is negligible in the general case ($\alpha \sim 1$, uppermost solid curve in each model), which have roughly $\sim 0.1 M_\odot$ (over 4π) of overlying envelope. For jet and shock radii occurring further in, as in the lower of each set of curves, the overlying envelope material that we took is more massive, $\sim 1 M_\odot$. In this case the absorption effects can become noticeable, especially in He models,

and this might serve as a diagnostic of the sub-surface jet depth (or the overlying material). For a solar mass above the jet head (distributed over 4π), the optical depth for νN interactions becomes larger than unity at energies $E_\nu \gtrsim 2.5 \times 10^{11}$ GeV in the H case and $E_\nu \gtrsim 2.5 \times 10^5$ GeV in the He case (seen as a cut-off in the lower set of He curves). Typically 80% of the ν -energy is transferred to the secondary lepton: e or μ . These μ 's further decay to ν 's, however, they are subject to severe synchrotron and inverse Compton losses and do not contribute substantially to lower energy flux.

The diffuse fluxes are based on a conservative estimate of the source density from the observation that $\sim 10^3$ GRB are known to occur per year over the entire sky, based on γ -ray detections. If these are attributed to massive stellar collapses, each GRB should be preceded by neutrino precursor events, starting tens of seconds (typically ~ 30 s [8]) before the γ -rays. The total ν_μ diffuse flux from all of these (γ -ray quasi-coincident) events is given by the solid curves in Fig. 1. (Considering mass-mixing along the way to Earth from $z \sim 1$, the ratio of flavors as observed from earth should become unity). The number of neutrino bursts and correspondingly the diffuse neutrino flux may be up to a factor $100q$ higher than what is shown in Fig. 1, if the ratio of the number of buried jets which do not emerge (γ -ray dark bursts) to that of those which do emerge is $100q$, where $q \lesssim 1$.

The number of muon neutrino events, in a km^2 detector (IceCube [14] e.g.), from a single GRB at redshift $z = 1$ with buried jet of duration $\Delta t \approx 30$ s is 0.6 and 0.003 in the $r_{12.5}$ (H) and in the r_{11} (He) cases, respectively, in the 1-100 TeV energy range. The number of events can be significantly larger for brighter ($L_\gamma^{iso} > 10^{52}$ ergs/s) or nearer ($z < 1$) bursts, or also if they are of longer duration ($\Delta t > 30$ s).

VII. IMPLICATIONS

The main feature of the high energy neutrino spectra of massive stellar collapse buried jet models related to GRB (and also of models involving a precursor supernova, Refs. [10, 15]), is that a “thicker target” of nucleons and photons is available to give higher fluxes of ~ 1 -100 TeV neutrinos, compared to those expected from internal or external shocks which occur outside the stellar progenitor [4, 9].

The neutrino flux expected in association with electromagnetically detected GRB, shown in Fig. 1, precedes the γ -rays by about 10-100 seconds, approximately the time taken by the jet to emerge from the collapsing core and the stellar envelope. Neutrinos coming from both $p\gamma$ and pp interactions in the sub-stellar jet are heavily suppressed by inverse Compton scatterings due to large photon density. The precursor neutrinos in the 1-100 TeV range from a single γ -ray bright event, coming from pp interactions in the H envelope ($r_{12.5}$ case) can be detected with ICECUBE. The number of events from a sin-

gle burst at a distance $D = 10^{28.2}$ cm ($z \sim 1$) and duration $\Delta t = 100$ s would be ~ 4 in the $r_{12.5}$ H-envelope star case, compared to $\lesssim 0.04$ in the r_{11} He star case. (Rare single bursts occurring about once per year at $D \sim 10^{27.2}$ cm could yield $\sim 10^2$ higher event rates per burst). Thus, detection of many bursts with 1-100 TeV neutrino precursors in correlation with a subsequent γ -ray detectable GRB would be a strong indication for an H progenitor. A rare detection of a weaker 100 TeV neutrino precursor would favor a He star progenitor.

The number of stars more massive than about 30 solar masses out to $z \sim 1$ undergoing a core collapse that leads to a black hole is about 10^7 /year corresponding to $\sim 3 \times 10^{-2}$ yr $^{-1}$ galaxy $^{-1}$ of type II supernovae rate. An interesting possibility [5] is that many or perhaps all of these lead to jets as in GRB, in which case most of these jets do not break through the stellar surface, and hence are not observed in γ -rays (at most $\sim 10^3$ /year can be observed as GRB). If the mean jet solid angle subtends 1% of the sky, this means $\lesssim 10^5$ /year such γ -ray dark (choked) bursts whose jets are directed at earth. These would be detectable only through their neutrino emission, which should be the same per burst as for the γ -ray bright bursts, but they would be up to 100 times more numerous. The diffuse ν_μ flux from these γ -ray dark collapses would be similar to that of the γ -ray bright solid neutrino curves of Fig. 1, but up to 100 times higher.

The diffuse neutrino signals from both γ -ray bright and dark collapses should be detectable with IceCube, as can be seen from the sensitivity curves in Fig. 1. For the γ -ray bright case plotted, the TeV-PeV flux detection is aided by the positional and temporal coincidences with electromagnetic detections. The typical angular resolution of planned neutrino telescopes at TeV energies [14] should be $\theta \lesssim 1^\circ$. For the γ -ray dark cases, the diffuse flux for a total number of collapses $\lesssim 10^5$ /year out to $z \sim 1$ would be sufficiently above the atmospheric

neutrino background, especially in the PeV range, that detection appears possible even without coincident photon flashes. (The γ -ray dark collapses could, however, be possibly associated with faint supernova-like optical/IR events, weeks to months later, if the stellar envelope is ejected).

The non-detection of a diffuse signal would be significant only if we have direct evidence for neutrino production in GRBs. This may come from a detection of either the GRB/afterglow neutrinos, or from a detection of the stellar pp neutrinos in the H case. In this case, an upper limit on the diffuse flux can serve to constrain the rate of “dark” bursts and the progenitor nature. If there is no direct evidence for neutrino production, the non-detection of a diffuse signal may imply no protons in the GRB jet and/or no proton acceleration.

The flux may exceed the WB bound [9] if opaque collisions occur where the pp ($p\gamma$) optical depth is very high, which implies that the nucleons do not escape. In this case, the proton energy generation rate of these “hidden sources” may exceed the energy generation rate inferred from cosmic-ray observations, and hence the neutrino flux may exceed the WB bound.

The neutrino flux level and spectra in detected GRBs would serve as a diagnostic of the outer dimensions of the stellar progenitor at the time the explosion occurred, providing useful constraints on the identity and evolutionary scenarios of the progenitors, as well as providing clues and a consistency check for possible association with supernova-like objects. The measurement of such neutrino bursts from γ -ray dark collapses would provide useful constraints on the total rate of massive stellar collapses at high redshifts, a quantity of significant interest for cosmological reionization, structure formation and intergalactic metal enrichment scenarios.

Acknowledgements- This work was supported in part by NSF AST0098416.

-
- [1] S. E. Woosley, W. Zhang & A. MacFadyen, *Astrophys. J.* in press [arXiv:astro-ph/0207436]
 - [2] P. Mészáros, *Ann. Rev. Astr. Astrophys.* **40**, 137 (Annual Reviews: Palo Alto) (2002).
 - [3] E. Waxman, *Phys. Rev. Lett.* **75**, 386 (1995).
 - [4] E. Waxman & J. N. Bahcall, *Phys. Rev. Lett.* **78**, 2292 (1997).
 - [5] P. Mészáros and E. Waxman, *Phys. Rev. Lett.* **87**, 171102 (2001) [arXiv:astro-ph/0103275].
 - [6] A. Beloborodov, B. Stern, R. Svensson, *ApJ*, 535, 158 (2000); E. Woods, A. Loeb, *ApJ* 453, 583 (1995)
 - [7] C.D. Dermer, *Astrophys. J.* 574:65, 2002.
 - [8] E. Waxman and P. Mészáros, *Astrophys. J.* **584**, 390 (2003).
 - [9] E. Waxman & J. N. Bahcall, *Phys. Rev. D* **59**, 3002 (1999).
 - [10] S. Razzaque, P. Mészáros and E. Waxman, arXiv:astro-ph/0212536.
 - [11] T. Sjostrand *et al.*, *Comp. Phys. Commun.* **135**, 238 (2001); T. Sjostrand *et al.*, arXiv:hep-ph/0108264.
 - [12] C.D. Dermer and A.M. Atoyan, astro-ph/0301030.
 - [13] Yu. Andreev *et al.*, *Phys. Lett. B* **84**, 247 (1979); D. McKay and J. Ralston *Phys. Lett. B* **167**, 103 (1986); G. Frichter *et al.*, *Phys. Rev. Lett.* **74** (1995), *Erratum-ibid.* **77**, 4107, (1996); R. Gandhi *et al.*, *Phys. Rev. D* **58**, 093009 (1998).
 - [14] IceCube Collaboration, J. Ahrens *et al.* astro-ph/0305196.
 - [15] J. Granot and D. Guetta, arXiv:astro-ph/0211433; D. Guetta and J. Granot, arXiv:astro-ph/0212045.